Weather and Climate Extremes 30 (2020) 100282

Contents lists available at ScienceDirect

Weather and Climate Extremes

journal homepage: http://www.elsevier.com/locate/wace

Could crop albedo modification reduce regional warming over Australia?

Jatin Kala [a,b,*], Annette L. Hirsch [b,c]

[a] Environmental and Conservation Sciences and Centre for Climate Impacted Terrestrial Ecosystems, Harry Butler Institute, Murdoch University, 6150, WA, Australia
[b] Australian Research Council Centre of Excellence for Climate Extremes, University of New South Wales, NSW, Australia
[c] Climate Change Research Centre, University of New South Wales, NSW, Australia

A B S T R A C T

Climate observations and projections for Australia show an increase in warm temperature extremes, including the frequency, duration and intensity of heatwaves. Recent global scale studies have suggested that agricultural land-use management options, such as increasing crop albedo, could reducing local warming. Australia has approximately 3,727,210 km^2 of cropland agricultural land-use, the majority of which is in southwest Western Australia and southeast Australia. This presents a potential opportunity to reduce regional warming via crop albedo enhancement. We use a regional climate model at 10 km resolution, to show that crop albedo enhancement of up to 0.1 could reduce monthly mean daily maximum temperatures by −1.0 °C to −1.2 °C, and monthly highest maximum temperatures by up to −1.4 °C to −1.6 °C during the cropping season. This cooling is approximately 3 times higher over Australia than global climate models predict. We highlight stronger cooling over southwest Western Australia as compared to southeast Australia, the opposite to global model studies which poorly resolve southwestern agricultural regions. The regional cooling was driven by a reduction in surface net shortwave radiation leading to a decrease in both sensible and latent heat flux of up to 50 W m^{-2} and 20 W m^{-2} respectively, when albedo is increased by up to 0.1. There were no cloud feedbacks or effects on precipitation. Our results highlight the importance of using regional climate models at a sufficiently high spatial resolution when investigating agricultural land-use management to reduce regional warming.

1. Introduction

The Paris agreement aims to "*to strengthen the global response to the threat of climate change by keeping a global temperature rise this century well below 2°C above pre-industrial levels and to pursue efforts to limit the temperature increase even further to 1.5°C*". Under current rates of warming, a global mean temperature increase of 1.5 °C relative to pre-industrial levels is expected to be reached between 2030 and 2052 (Allen et al., 2018), or perhaps earlier depending on the phase of large-scale modes of climate variability such as the Interdecadal Pacific Oscillation (Henley and King, 2017). The impacts of global warming of 1.5 °C versus 2.0 °C for Australia include a reduction in the frequency of extreme heat events by 25% at lower levels of warming (King et al., 2017). These extreme heat events have very significant impacts on human health (e.g., Peng et al., 2011), infrastructure (e.g., McEvoy et al., 2012), and marine and terrestrial ecosystems (e.g., Ruthrof et al., 2018). Additionally, climate projections show that the frequency, intensity and duration of extreme heat events across Australia is projected to increase in the future (Cowan et al., 2014), exacerbating an observed trend in in extreme heat and heatwaves (Perkins-Kirkpatrick et al., 2016; Perkins et al., 2012). Irrespective of the success of reducing greenhouse gas emissions, Australia is likely to experience more temperature extremes over the coming decades, highlighting the urgent need to develop effective climate adaptation and mitigation strategies.

The current rate of global warming is 0.2 °C per decade above pre-industrial levels (Allen et al., 2018), and current mitigation measures to reduce global greenhouse gas emissions have so far proven inadequate in slowing the rate of global warming (Friedlingstein et al., 2014; Rogelj et al., 2016). As a result, there has been significant discussion on two broad techniques to reduce warming, which are commonly referred to as geo-engineering. One is to remove carbon-dioxide from the atmosphere artificially (Mac Dowell et al., 2017). The other is to alter the radiative energy balance of the earth, often referred to as solar radiation management (SRM), to decrease the absorption of solar radiation at the Earth's surface (e.g., Keith, 2000; Irvine et al., 2016). Examples of SRM techniques which aim at reducing warming globally, i.e., large-scale SRM, include the emission of stratospheric aerosols, and marine cloud brightening (e.g., Vaughan and Lenton, 2011). The effectiveness of these proposed measures have been assessed using idealized simulations with earth system models, for example, the Geoengineering Model Intercomparison (GeoMIP) project (Kravitz et al., 2011). Results show that these SRM techniques could theoretically reverse warming associated with a 4-fold increase in atmospheric carbon dioxide, however, considerable uncertainties remain about un-intended negative impacts

* Corresponding author. Australian Research Council Centre of Excellence for Climate Extremes, University of New South Wales, NSW, Australia.
E-mail address: J.Kala@murdoch.edu.au (J. Kala).

https://doi.org/10.1016/j.wace.2020.100282
Received 23 December 2019; Received in revised form 28 August 2020; Accepted 31 August 2020
Available online 4 September 2020

and consequences, such as impacts on the hydrological cycle (e.g., Dagon and Schrag, 2016) and agricultural productivity (e.g., Pongratz et al., 2012), as well as termination effects if SRM were implemented and suddenly stopped (e.g., Parker and Irvine, 2018). Other significant challenges with large-scale SRM include governance, costs of remediation of unintended negative impacts and intergenerational justice, as well as the significant infrastructure and maintenance costs of large-scale deployment of SRM (e.g., Robock et al., 2009; Goes et al., 2011). As a result, large-scale SRM remains highly contentious (e.g., Preston, 2013).

Land based SRM techniques on the other hand, have been argued to be significantly more cost effective, as these do not share the inherent disadvantages of large-scale SRM (e.g., Seneviratne et al., 2018). The aim of these techniques is to use existing agricultural croplands, which account for approximately 35%–40% of global land use (Ramankutty et al., 2008), to increase the albedo of the land surface. Costs associated with land-based SRM are significantly lower as these land areas are already managed. Indeed, existing practices can be altered to increase crop albedo by using different varieties, adopting conservative agriculture via no-till farming to keep darker organic materials below the ground (and hence increase the albedo of the surface), use of irrigation for cooling, as well as other management approaches. These techniques have been the subject of numerous studies (Davin et al., 2014; Doughty et al., 2011; Hirsch et al., 2018, 2017; Seneviratne et al., 2018; Wilhelm et al., 2015) and they broadly conclude that land-based SRM has little impact on the global mean temperature, but can be an effective method to achieve regional cooling. These regional effects can be viewed as an advantage as it removes the issues associated with unintended remote impacts and does not require global governance structures as with large-scale SRM.

Cropland agriculture is a key component of the Australian economy, with approximately 3,727,210 km^2 used for agricultural production in 2016–2017, including land for crops, grazing, forestry and other agricultural purposes (Australian Bureau of Statistics, 2018). This agricultural land is mostly divided into two key regions, the wheat-belt of southwest Western Australia and the Murray-Darling Basin in southeast Australia, which comprise approximately 50% each of Australia's total cereal crop production (Australian Bureau of Statistics, 2008; Wilkinson, 2019). These large areas of managed agricultural land-use offer an ideal opportunity to investigate the potential for crop albedo modification to reduce regional warming for Australia, and potentially mitigate against impacts of future warming.

Studies using global earth system models typically do not represent agricultural land-use over the Australian continent adequately due to the relatively coarse resolutions of these models. For example, Ridgwell et al. (2009) investigated the impact of increasing crop albedo globally by 0.02, 0.04 and 0.08 using the HadCM3 model which has a 2.5° by 3.75° degree resolution. They showed cooling of up to 1 °C could be achieved in the northern hemisphere, but showed little to no change in the southern hemisphere. Wilhelm et al. (2015) conducted simulations using the CESM model, which has a resolution of 1.9° by 2.5° degrees by increasing the albedo over all vegetated surfaces by 0.05, 0.10, 0.15 and 0.20 over all vegetated surfaces. They showed preferential cooling of hot extremes, especially in the northern midlatitudes during the boreal summer. Hirsch et al. (2017) expanded on the work of Wilhelm et al. (2015) by using the CESM model at a resolution of 1.9° by 2.5° degrees, but focused on crop albedo enhancement and irrigation. They showed that crop albedo enhancement with irrigation was able to reduce warming by more than 2 °C in North America, Eurasia and India, and changes over the Australian continent were small and not statistically significant.

An issue with all of the above studies is that at such coarse resolutions, the agricultural regions over Australia are poorly represented, especially the southwest of Western Australia which is only represented by 2–3 grid cells. Additionally, these studies tend to focus on the boreal summer period (June-July-August), whereas the cereal cropping season

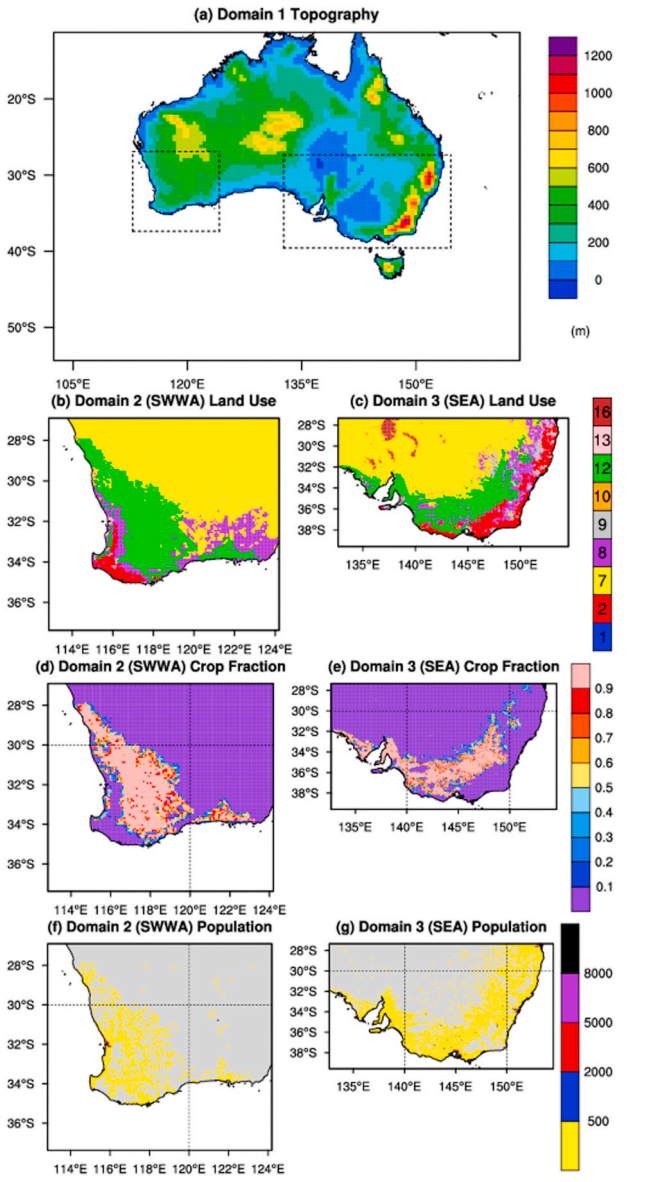

Fig. 1. (a) Model topography (m) for domain 1 and boundaries of domains 2 (SWWA) and 3 (SEA) shown by dotted lines, (b–c) dominant land use category for domains 2 (SWWA) and 3 (SEA), (d–e) crop fractions for domains 2 (SWWA) and 3 (SEA), (e–f) population for domains 2 (SWWA) and 3 (SEA). Land-use categories in b-c follow the International Geosphere–Biosphere Programme (IGBP) as used in WRF for the Noah land surface model (1-Evergreen Needleleaf forest, 2-Evergreen broadleaf forest, 7-Open Shrublands, 8-Woody Savannas, 9-Savannas, 10-Grasslands, 12-Croplands, 13-Urban and Built-up, 16-Barren or sparsely vegetated). The population data shown in (e) and (f) is from the Australian Bureau of Statistics population data interpolated to the WRF domain. This is not used by the model, but shown here for illustration for results averaged across population densities shown later in the manuscript.

in southern parts of Australia when crops are growing and photosynthetically active is generally between July to October. Few studies have used regional climate models (RCMs) to investigate the potential for land-based SRM in reducing warming at the regional scale, however, to the best of our knowledge, these have all focused on the northern hemisphere (e.g., Davin et al., 2014). The few recent studies which have used RCMs to investigate land-based SRM in Australia have focused on urban land-use management (Imran et al., 2019, 2018; Jacobs et al., 2018; Ma et al., 2017), rather than agricultural management.

In this paper, we present the first study to examine the potential for crop albedo enhancements in Australia to reduce hot extremes during

Table 1
WRF physics ensemble used in this study for the Planetary Boundary Layer (PBL), Surface Layer (SL), and Cumulus schemes. YSU is the Yonsei University PBL scheme, MYJ is Mellor-Yamada-Janjic PBL scheme, MO is Monin-Obukhov similarity, KF is the Kain-Fritsch scheme, and BMJ is the Betts-Miller-Janjic cumulus scheme.

Ensemble	PBL/SL scheme	Cumulus scheme
ENS1	YSU/MO	KF
ENS2	MYJ/ETA	KF
ENS3	YSU/MO	BMJ

the cropping season, using a regional climate model at a resolution of 10 km which can adequately represent the key agricultural regions of Australia. Idealized simulations are carried out by increasing crop albedo during the growing season, to determine the maximum cooling benefits which could potentially be achieved if large-scale changes in agricultural practices were to be altered to increase crop albedo.

2. Methods

2.1. Study region

This study focusses on the two key agricultural regions of Australia, the southwest of Western Australia (SWWA), and southeast Australia (SEA) (Fig. 1). SWWA experiences a Mediterranean climate with cool and wet winters and hot and dry summers (Gentilli, 1971). The region is one of Australia's key regions of cereal crop production, with significant wheat production generating approximately 50% of Australia's total wheat production, generating $2–3 billion for the Western Australian State economy each year (Wilkinson, 2019). Agriculture in SWWA is rain-fed with no irrigation and hence the growing season is based around the wet winter season. Regional climate projections for SWWA show an overall statistically significant increase in both maximum and minimum temperature across all seasons and a decline in winter rainfall (Andrys et al., 2017). SEA experiences a more temperate climate compared to SWWA, with no clearly defined dry season, but hot summers (Gentilli, 1971). The region has two of the longest rivers in Australia and covers more than 1 million square kilometres. In contrast to SWWA, both dryland (rain-fed) farming and irrigation are used, with irrigation mostly used for dairy farming and cotton growing. Similar to SWWA, agriculture in SEA accounts for approximately 50% of total grain production in Australia, which is mostly comprised of wheat, followed by barley.

2.2. Model description and experiments

We use the Weather Research and Forecasting (WRF) (Skamarock et al., 2019) version 4.0.2, a state-of-the-art and widely used regional atmospheric modelling system. The WRF model has been extensively used and evaluated for multi-decadal regional climate model simulations over Australia (Andrys et al., 2015; Di Virgilio et al., 2019; Evans and McCabe, 2010; Firth et al., 2017; Kala et al., 2020), as well as the simulation of extreme heat events (Hirsch et al., 2019a; Kala et al., 2015b). The model was configured with three nested domains as illustrated in Fig. 1. The outer domain has a resolution of 50 km, and the two inner nests have resolutions of 10 km each, and cover the two main agricultural regions of Australia; SWWA (domain 2) and SEA (domain 3). All simulations were driven with 6 hourly lateral boundary conditions from ERA Interim re-analysis (Dee et al., 2011) and simulations were carried out for 6 years from June to October, including El Niño, La Niña, and neutral periods (1983-La Niña, 1994-El Niño, 1997-El Niño, 1998-La Niña, 2008-Neutral, 2010-La Niña).

All simulations were carried out using the Noah land surface model (Chen and Dudhia, 2001), which is the most commonly used and extensively evaluated land surface model in WRF. Given that WRF is sensitive to physical parameterization options over both SEA and SWWA (Evans et al., 2012; Hirsch et al., 2019b; Kala et al., 2015a), we ran three ensembles to sample model structural variability (Table 1) based on these studies. The first ensemble used the Yonsei University planetary boundary layer (PBL) scheme with Monin-Obukhov similarity for the surface layer (Hong et al., 2006), the Rapid Radiative Transfer Model (RRTM) scheme for longwave radiation (Mlawer et al., 1997), the Dudhia scheme for shortwave radiation (Dudhia, 1989), and the Kain-Fritsch scheme for convection (Kain, 2004). The second ensemble differs from the first by using the Mellor-Yamada-Janjic PBL scheme with ETA scheme for the surface layer (Janjić, 1994), and the third ensemble differs from the first ensemble by using the Betts-Miller-Janjic scheme for convection (Betts and Miller, 1986). We do not carry out additional model evaluation against observations in this paper, as all these WRF configurations, which all use the Noah land surface model, have already been extensively evaluated over both SEA and SWWA by numerous studies against maximum and minimum temperature and precipitation observations, and shown to reproduce the observed climatology reasonably well (Andrys et al., 2016, 2015; Di Virgilio et al., 2019; Evans et al., 2012; Evans and McCabe, 2010; Firth et al., 2017; Hirsch et al., 2019a, 2019c; Kala et al., 2015a).

Table 2
Minimum and maximum crop albedo for all WRF simulations.

Experiment	Minimum Crop Albedo	Maximum Crop Albedo
CNTL	0.17	0.23
+0.02	0.19	0.25
+0.04	0.21	0.27
+0.06	0.23	0.29
+0.08	0.25	0.31
+0.10	0.27	0.33

Simulations were carried out between June and October, with the first month discarded as spin-up and outputs analyzed from July to October (the growing season in Australia). All WRF simulations were configured to use albedo values for the different vegetation categories based on look-up tables rather than the use of climatological monthly mean albedo derived from remote sensing, which is more commonly used for the long-term regional climate simulations. Following Hirsch et al. (2017) and previous studies which have investigated albedo enhancement (Wilhelm et al., 2015), idealized experiments were carried out by increasing the albedo of crops by 0.02, 0.04, 0.06, 0.08 and 0.10 (Table 2). As discussed in Hirsch et al. (2017), variations in albedo typically range between 0.01 to more than 0.1 for different cultivars of the same crop type. This can arise from various differences in leaf attributes in addition to contributions from the background soil type and moisture content when scaled from leaf-level to ecosystem scales. Observational studies measuring the variation in leaf-level crop albedo include albedo variations of 0.01–0.06 across barley cultivars (Breuer et al., 2003; Febrero et al., 1998), 0.02 across soybean cultivars (Breuer et al., 2003), 0.05 across sorghum cultivars (Grant et al., 2003), 0.06 to 0.1 in wheat cultivars (Uddin and Marshall, 1988), 0.08 to 0.1 across maize, sunflower and oat cultivars (Breuer et al., 2003; Hatfield and Carlson, 1979) and 0.14 for rye cultivars (Breuer et al., 2003). Therefore, variations in crop albedo across the increments tested here reflect plausible changes within crop cultivars, and do not necessarily imply changing the crop species grown which may affect food production.

The default minimum and maximum albedo for the Croplands land use category used by the Noah land surface model in WRF are 0.17 and 0.23 respectively. The actual albedo is taken as 0.5*minimum albedo +0.5*maximum albedo. For the largest perturbation (+0.10), this leads to albedo values of 0.3. These values are within ranges of observed albedo of wheat and barley in Australia, with past field observations reporting values of daily albedo ranging from 0.13 to 0.25 for wheat and from 0.14 to 0.36 for barley in southeast Australia (Piggin and Schwerdtfeger, 1973). In summary, a total of 108 simulations were

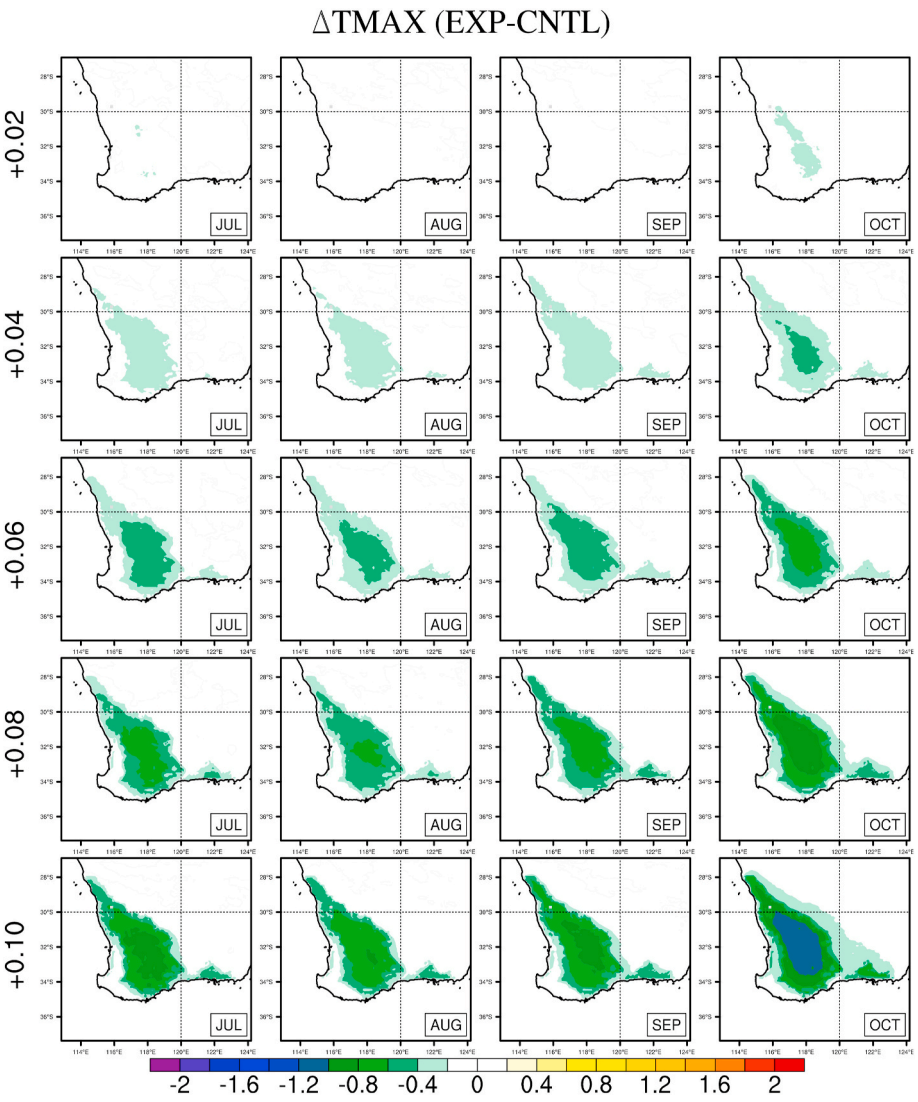

Fig. 2. Change (Experiment (EXP) minus Control (CNTL)) in monthly mean maximum temperature (TMAX, °C) in SWWA (domain 2) between the experiments with enhanced crop albedo by 0.02, 0.04, 0.06, 0.08, and 0.10 respectively and the control simulation. Results are averaged across all 6 years and across all 3 WRF ensembles (Table 1).

carried out (i.e., for 6 years, each of which had 1 control simulation and 5 experiments with increasing crop albedo from 0.02 to 0.10 (Table 2), resulting in 36 simulations, with 3 ensembles, making a total of 108 simulations).

We note that we did not sample internal model variability by running additional WRF simulations with slightly different initial conditions. Recent work has shown that for very short WRF simulations (model initialized 1 day before the event(s) of interest), internal model variability can be comparable to the effect of structural variability (use of different physics options), but for longer simulations (several years), this becomes less important (Lavin-Gullon et al., 2020). Given the relatively large number of simulations (108), it was not possible to carry out further ensembles with different initial conditions. However, since we ran 6-month simulations and discarded the first simulation month, we are confident that this is long enough that effects of model structural variability would be more important than effects of internal variability. Indeed, recent work comparing WRF simulations over Australia, using the same version but with different physics options, has shown that the choice of radiation option can have a very large impact on simulated temperatures. Additionally, this work has also showed that different versions of WRF had overall similar performance as compared to two other regional climate models (Di Virgilio et al., 2019). This provides us with confidence in our choice of model, as well as our experimental design with three different WRF physics set-ups.

2.3. Analysis

We show results as monthly means, averaged over the 6 years, and across the 3 ensembles, unless otherwise stated, and only show results for domains 2 and 3 over SWWA and SEA respectively (Fig. 1 (b) and (c)), which have 10 km resolution. We first show changes in mean and highest monthly maximum temperature between the experiments and the control. To examine the drivers of the changes, daily maximum temperatures at each grid cell are sorted to extract the 1st, 5th, 10th, 30th, 50th, 70th, 90th, 95th, and 99th percentiles. For every daily maximum temperature, the hour of occurrence was also saved, and corresponding variables (e.g., sensible heat flux, latent heat flux, incoming and outgoing radiation etc) were extracted at the same hour to examine the mechanisms. Changes between the experiments and control were calculated for each percentile and plotted as median changes, only for grid cells with greater than 60% cropland, with the interquartile range used to quantify spatial variability in the changes.

We also use the land-atmosphere coupling metric derived from Dirmeyer (2011) to focus on the covariance of sensible heat flux (HFX) and

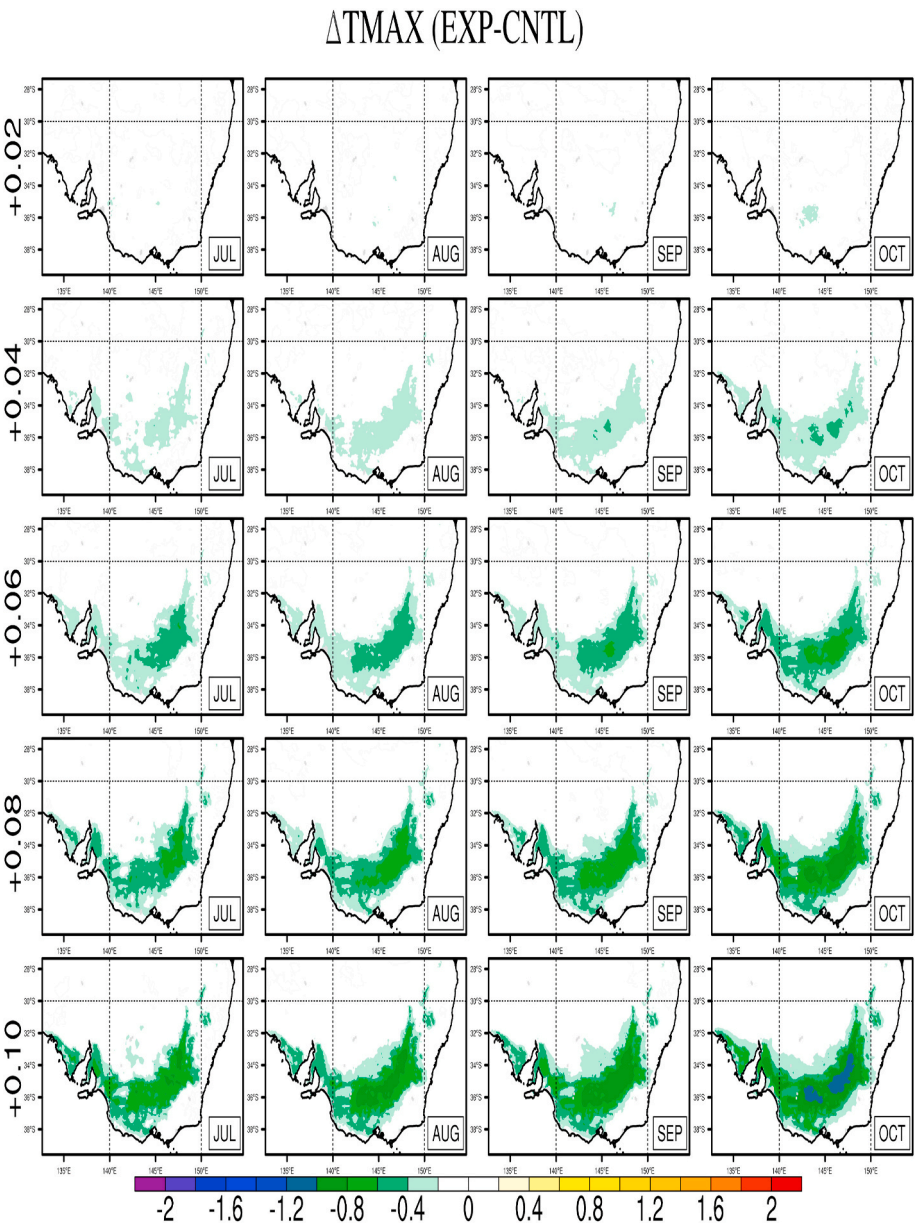

Fig. 3. Same as in Fig. 2 expect for SEA (domain 3).

maximum temperature (TMAX) as follows:

$$I_A = \frac{\sum\left(HFX - \overline{HFX}\right)\left(TMAX - \overline{TMAX}\right)}{\sqrt{\frac{1}{N}\sum\left(HFX - \overline{HFX}\right)2}} \quad (1)$$

HFX here is the sensible heat flux at the hour that TMAX occurs. $\overline{HFX}$ and $\overline{TMAX}$ denotes the climatological means for a particular day of the year, and computed from the control simulations, and TMAX and HFX are the daily values from the experiments. N is the number of days over which I_A is computed, and in this paper, we compute I_A over a monthly time-scale. Positive I_A values imply that changes in HFX drive changes in TMAX and denote a "land-driven" regime, whereas negative values denote an "atmosphere-driven" regime. Following Hirsch et al. (2019a), I_A values are normalized by subtracting the spatial mean and dividing by the spatial standard deviation for ease of interpretation, and values greater than 0.2 denote strong land-atmosphere coupling.

3. Results and discussion

3.1. Effect of increasing crop albedo

Figs. 2 and 3 show the mean monthly difference in maximum temperature (experiment minus control) for each experiment, averaged across all ensembles and years for SWWA and SEA respectively. There are negligible changes in TMAX when crop albedo in increased by 0.02, and cooling gradually increases by up to −1.0 °C to −1.2 °C as crop albedo is increased by up to 0.10. The magnitude of cooling increases from cooler (July) to warmer (October) months, which is expected given higher solar radiation during summer. The magnitude and spatial extent of cooling is generally larger for SWWA as compared to SEA, and this is especially noticeable in October for experiment +0.10, with a much larger area of SWWA showing of up to −1.0 °C to −1.2 °C. The pattern of cooling in both regions are coherent and match the changes in albedo, and are limited in geographical extent to the regions of albedo increase.

Figs. 4 and 5 are the same as Figs. 2 and 3, but show changes in the highest monthly maximum temperature. The overall results are similar

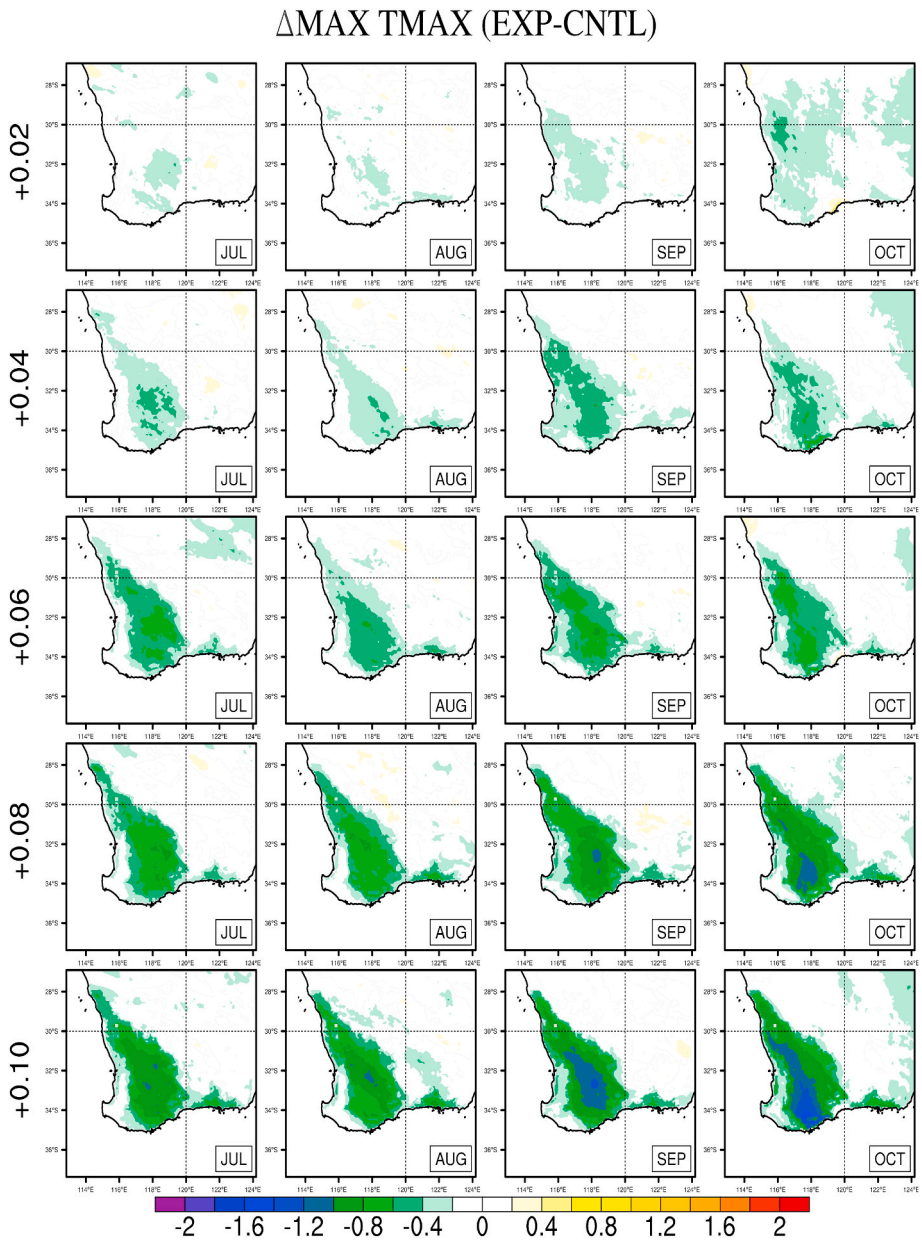

Fig. 4. Same as in Fig. 3 except showing the change in highest monthly maximum.

to the changes in the mean maximum, but with larger reductions of up to −1.4 °C to −1.6 °C as well as relatively small areas outside of the agricultural regions (Fig. 1) showing slight increases of up to 0.4 °C–0.6 °C, especially for experiments with lower increases in crop albedo. This is associated with higher variability when considering changes in the monthly highest daily maximum as compared to the mean daily maximum. Differences in mean maximum temperature varied between different years, especially for SEA, which is a region strongly modulated by El Niño Southern Oscillation (ENSO), with strong El Niño conditions generally resulting in hotter and drier conditions, and strong La Niña years generally leading to wetter conditions. This is illustrated in Figs. S1 and S2, showing that differences were generally larger in 1994 (a strong El Niño year) versus 2010 (a strong La Niña year), showing that crop albedo modification is effective during periods when hotter than average conditions are expected. Differences between years were not as large for SWWA as compared to SEA (not shown). This is expected given that correlations between phases of ENSO and temperature and precipitation is much weaker in SWWA as compared to SEA where correlations are generally stronger. Variations between the 3 ensemble members are illustrated in Figs. S3 and S4 showing the change in mean maximum temperature for October for the +0.10 experiment (month and experiment with highest change) averaged over the 6 years, for SWWA and SEA respectively. ENS2 shows a larger response as compared to ENS1 and ENS3 for both SWWA and SEA, whereas ENS1 and ENS3 show broadly similar responses, with ENS1 only showing a slightly higher response as compared to ENS3. ENS1 and ENS3 differ in the choice of cumulus scheme (Table 1), and since there was little to no change in convective precipitation (not shown), it is not surprising that the changes in mean maximum temperature between these two ensembles was small. ENS2 and ENS1 differ in the choice of boundary-layer scheme, and ENS2 and ENS3 differ in the choice of boundary-layer and cumulus scheme (Table 1), showing that the choice of PBL scheme can strongly modulate the maximum temperature response. This is consistent with previous studies using the WRF model, which have shown the impacts of land-use change on temperature extremes in Australia, can be strongly dependent on choice of PBL scheme in WRF

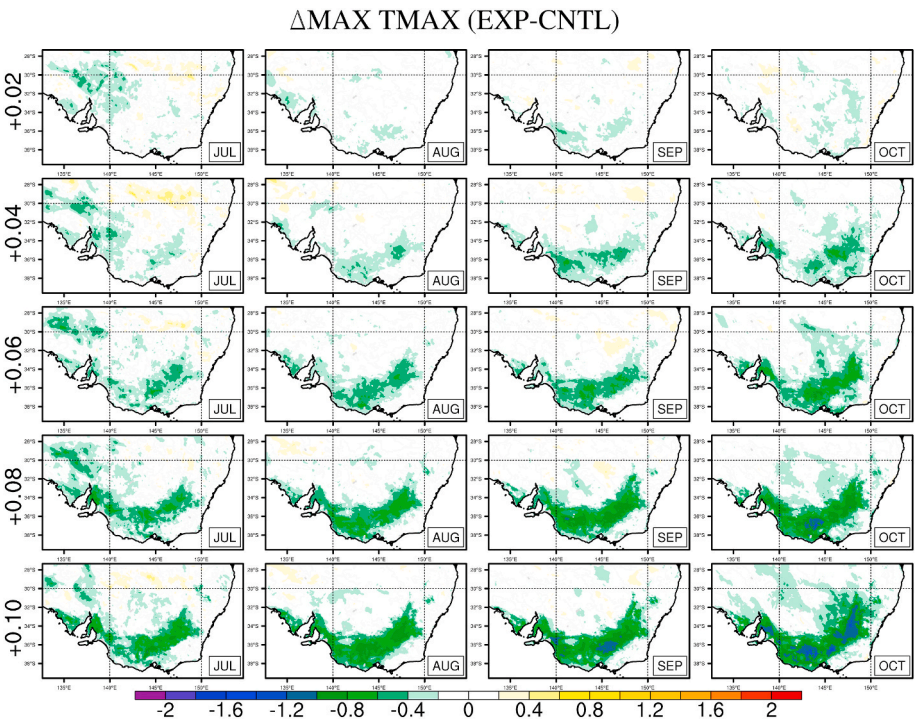

Fig. 5. Same as in Fig. 4 except showing the change in highest monthly maximum.

(Hirsch et al., 2015a).

3.2. Cooling mechanism

To investigate the mechanisms that explain the cooling, we examine changes in the different percentiles of maximum temperature and associated changes in key surface energy balance components (refer to section 2.3 in the Methods section). This is shown in Fig. 6 showing the median changes in TMAX for each percentile (1st, 4th, 10th, 30th, 50th, 70th, 90th, 95th and 99th), and corresponding changes in net shortwave (SWNET), longwave (LWNET), sensible (HFX) and latent (LH) heat flux with the interquartile range shown as dotted vertical lines to show spatial variability. These results are averaged over grid cells with crop fraction greater than 60% only. SWNET was computed as incoming solar radiation multiplied by 1 minus the albedo. For LWNET, downwelling longwave radiation at the surface was obtained directly from WRF outputs and upwelling longwave radiation was computed using surface temperature and emissivity from WRF outputs.

Fig. 6 shows that generally, reductions in TMAX percentiles are larger for SWWA as compared to SEA, especially for experiments with larger increases in crop albedo. The corresponding changes in SWNET show a reduction of up to 70–80 W m^{-2} for the +0.10 experiment, as expected. The increase in LWNET of up to 10–12 W m^{-2} was due to the decrease in surface temperature resulting in a decrease in upwelling longwave radiation (and therefore an increase in LWNET). Median changes in downwelling longwave radiation were small ranging from −3 to 3 W m^{-2} with no clear pattern (not shown) and changes in surface emissivity were negligible (not shown). The overall decrease in net radiation (SWNET plus LWNET) translates in a median decrease in HFX and LH of up to 40–50 W m^{-2} and 15–20 W m^{-2} respectively. The decrease in LH happens although there was an overall increase in surface soil moisture of 0.014 m^{-3} m^{-3} (Fig. S5) due to lower net radiation available to drive evapotranspiration. There were no cloud feedbacks with small and inconsistent changes in cloud fraction, incoming solar radiation and precipitation (not shown). The reduction in TMAX percentiles is largely driven by a reduction in net radiation, which reduces both latent and sensible heat fluxes, but does not affect the partitioning. This is illustrated in Fig. 7 showing the ratio of sensible to latent heat for SWWA and SEA respectively during October when changes where highest. The ratio remained the same for all experiments and the control, but only the magnitude decreased with increasing albedo perturbations, as shown by the scatter plots shifting to the left, going from the CNTL to the +0.10 experiment.

To examine remote effects, especially in densely populated urban and peri-urban regions where crop albedo perturbations are not possible, we also examined changes in the mean maximum and highest maximum averaged across grid cells with different population densities, obtained from the Australian Bureau of Statistics (Fig. 1(f and g)), as illustrated in Fig. 8. Although the largest reductions in TMAX and MAX TMAX occur in less densely populated regions of SEA and SWWA, reductions in MAX TMAX of approximately 0.3 °C can be obtained in the most densely populated regions, especially SWWA.

Reductions in maximum temperature were higher for SWWA as compared to SEA, as evident in Figs. 2–6 and 8, and the most likely explanation is the larger reduction in sensible heat flux for SWWA as compared to SEA (Fig. 6). To quantify this, we examine the land-atmosphere metric, I_A (Eq (1)), which is the covariance of the maximum temperature and the sensible heat flux at the hour that the maximum temperature occurs. This is illustrated in Fig. 9 showing contour plots of I_A for the +0.10 experiment for October (experiment with largest change) for SWWA and SEA respectively, only over grid cells with >0.6 crop fraction. I_A is higher in magnitude for SWWA as compared to SEA, and also higher over a larger area in SWWA as compared to SEA, which explains the stronger response. This is consistent with previous work examining land-atmosphere coupling strength over Australia which has also identified SWWA as a hot-spot and weaker coupling over SEA (Hirsch et al., 2019a, 2015b, 2014).

4. Summary and conclusions

Recent studies which have investigated the potential for altering land-use to reduce regional warming in Australia have typically focused on urban land-use, via the use of green and cool roofs, urban greening and irrigation (e.g., Imran et al., 2018, 2019; Jacobs et al., 2018). The

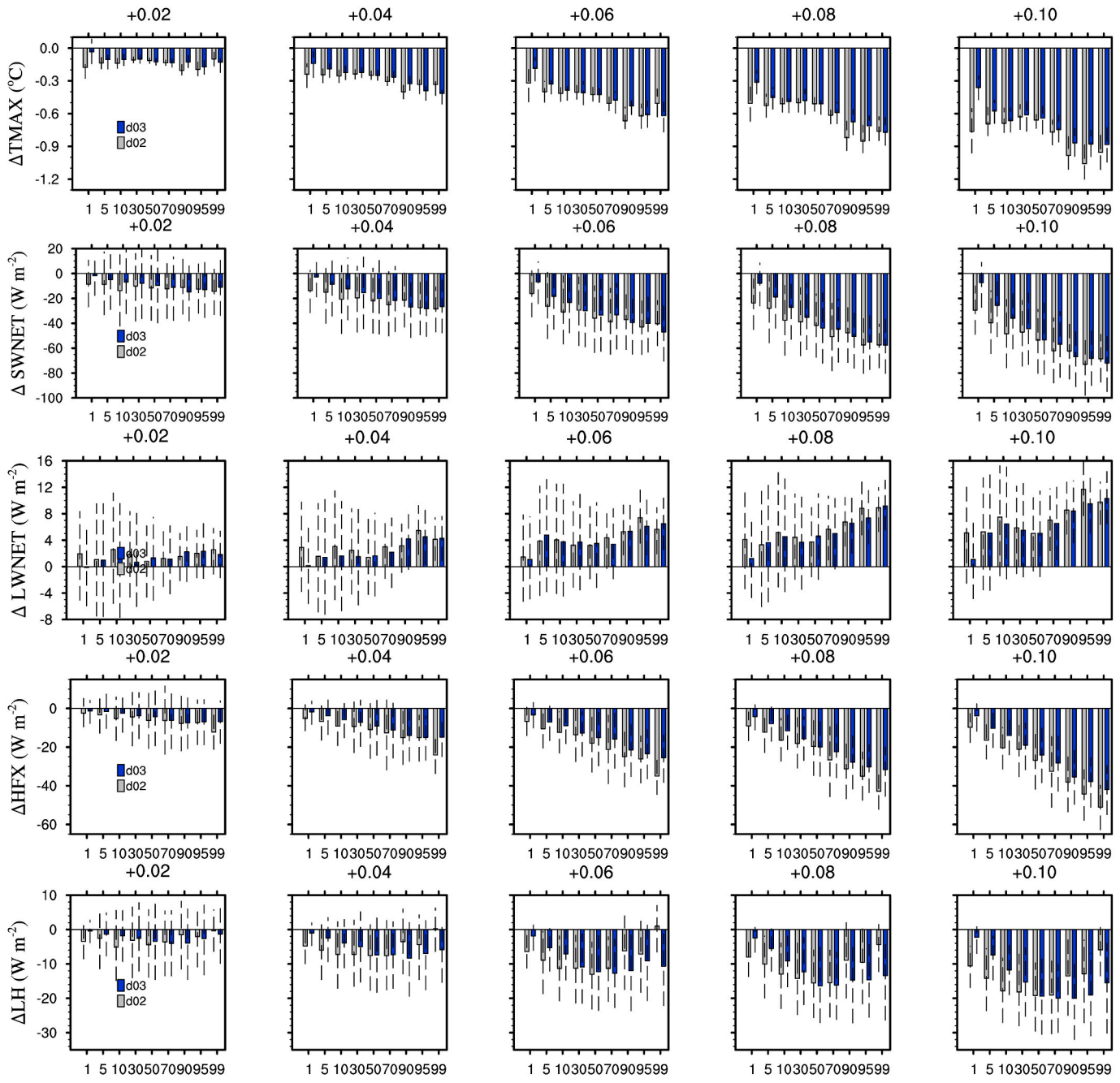

Fig. 6. 1st, 4th, 10th, 30th, 50th, 70th, 90th, 95th and 99th percentile median changes in TMAX (EXP-CNTL) and corresponding percentile changes in net shortwave radiation (SWNET), net longwave radiation (LWNET), sensible heat flux, and latent heat flux heat fluxes. Results are averaged across all grid cells with a crop fraction greater than 60% across domains 2 (grey for SWWA) and domain 3 (blue for SEA) respectively (refer to Fig. 1 for the extents of domains 2 and 3). Black dotted lines represent the interquartile range.

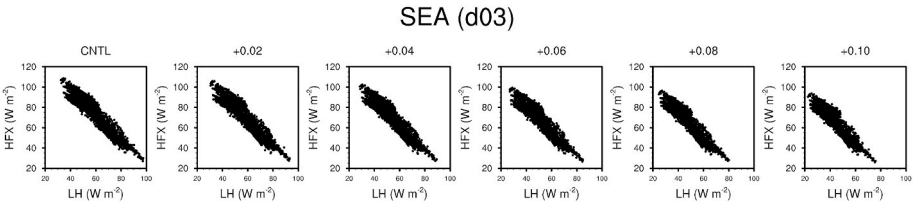

Fig. 7. Scatter plots of sensible (HFX) versus latent (LH) heat fluxes for the control (CNTL) and all experiments (Table 1) for October, for SWWA and SEA. Results are only shown over grid cells with greater than 60% crop fraction.

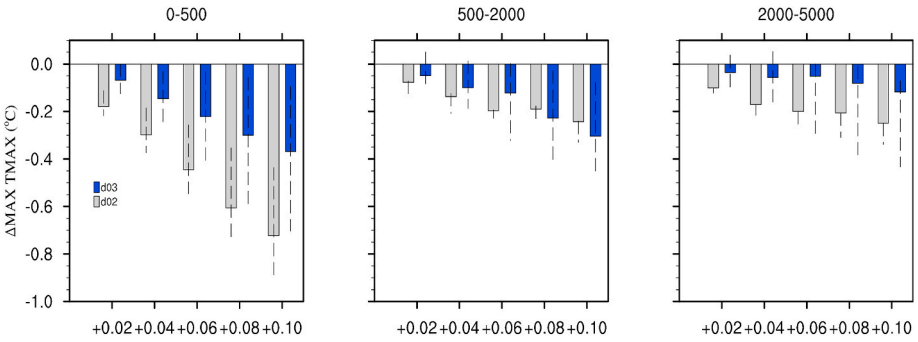

Fig. 8. Median changes (EXP minus CNTL) in mean maximum temperature (TMAX), and highest maximum (MAX TMAX) average across grid cells with populations of 0–500, 500–2000, and 2000–5 000 per square kilometre for each experiment (Table 2). Dotted black lines represent the interquartile range.

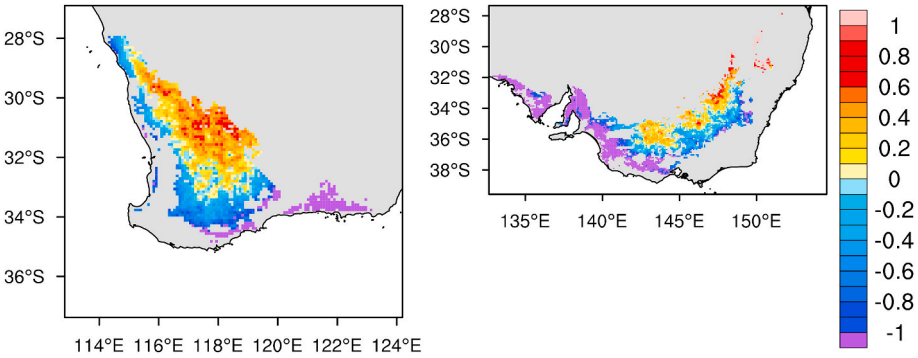

Fig. 9. Land-atmosphere coupling metric I_A (Eq (1)) for SWWA (left) and SEA (right) for the +0.10 experiment for October, averaged across all years and ensembles. Strong land-atmosphere coupling is defined as I_A greater than 0.2.

very large expanse of managed agricultural land-use in Australia presents an opportunity to investigate the potential for land surface radiation management at much larger spatial scales. However, all studies to date have used global models, with coarse spatial resolutions that are not able to adequately resolve the two key agricultural regions of Australia (Hirsch et al., 2017). We investigated for the first time, the potential for agricultural land use management to reduce regional warming via crop albedo enhancement at a 10 km resolution focusing, on the two key agricultural regions of Australia, SWWA and SEA.

We found that increasing crop albedo by 0.1 lead to reductions of −1.0 °C to −1.2 °C for the mean maximum, and −1.4 °C to −1.6 °C for the highest maximum. These reductions are approximately 3 times as large as compared to Hirsch et al. (2017) who report relatively small changes in the annual maximum temperature over the Australian continent of approximately −0.25 °C to −0.5 °C when crop albedo is increased by 0.1 (refer to Fig. 2(d) of Hirsch et al., 2017). There may be several reasons for this. At coarse GCM resolutions of 1.9° by 2.5° degrees in Hirsch et al. (2017), the crop fraction per grid cell will be small, and results averaged over the entire grid cell will inviably be smaller, as compared to RCM simulations at 10 by 10 km resolution. It is also possible that the Noah land surface model in WRF responds more strongly to albedo perturbations as compared to CLM in CESM in the study by Hirsch et al. (2017). Results from our domain 1 (not shown), which has 50 km resolution, as compared to the 10 km domains over SWWA and SEA, showed similar magnitudes of cooling, suggesting that at least part of the differences may be due to different land surface models, rather than resolution alone. Testing this would require running the same version of the CLM land surface model used by Hirsch et al. (2017) in WRF, however, this is outside the scope of this study.

Hirsch et al. (2017) classified SEA as a region whereby irrigation would be the preferred cooling mechanism, assuming unlimited water supply. Given drought conditions in SEA and large uncertainties for future water supply in this region (van Dijk et al., 2013), our results would suggest that albedo modification may well be a more realistic option. Our results also showed a stronger cooling response in SWWA as compared to SEA, a result which was not captured by Hirsch et al. (2017) due to a coarse longitudinal resolution of 2.5° which captured the cropping regions of SEA, but not SWWA. While studies using coarse resolution global climate models can be very useful, our results show that they can miss entire cropland regions whereby regional cooling can be achieved using land-based agricultural radiation management.

The magnitude of regional cooling for the monthly highest maximum ranged from −1.4 °C to −1.6 °C. This is a similar order of magnitude to the observed difference in maximum daily temperatures between El Nino and La Nina years in Australia (Arblaster and Alexander, 2012). Hence, by simply increasing crop albedo, we obtain changes which are comparable to the effects of natural climate variability. However, there are several caveats which need to be taken into consideration. Our simulations are idealized and designed to investigate the maximum possible response. Increasing crop albedo across such large areas is unlikely to be practical in reality for several reasons. Firstly, we did not consider different types of crops (e.g., wheat, barley, canola), which is a limitation of the model only having a generic crop type. Explicitly representation of particular crop types, e.g., winter growing wheat, is becoming more common in land surface models (e.g., Lu et al., 2017), and this would allow for more accurate representation. Additionally, we did not consider other key crop physiological parameters, such as water use efficiency. For example, crops with higher albedo and low water use efficiency may not be a viable option, especially under a drying climate. Finally, while the WRF model is widely used, all simulations used the same land surface model, and it is well documented from land surface model inter-comparison projects, that results from land-use change/-modification experiments can vary widely depending on the land surface model used within climate models (e.g., Boisier et al., 2012; de Noblet-Ducoudré et al., 2012). Hence, it would be worthwhile to test different land surface models, such as the Community Land Model

(CLM5), which is now available in WRF. Nonetheless, our results are encouraging, and show that agricultural land-surface radiation management could be a viable adaptation option for Australia. The larger cooling response over SEA during El Niño versus La Niña years, highlights the effectiveness of albedo enhancement at times when warmer than average conditions are expected.

CRediT authorship contribution statement

Jatin Kala: Conceptualization, Methodology, Software, Validation, Formal analysis, Investigation, Data curation, Writing - original draft, Writing - review & editing, Visualization, Project administration, Funding acquisition. **Annette L. Hirsch:** Conceptualization, Methodology, Investigation, Writing - original draft, Writing - review & editing.

Declaration of competing interest

The authors declare that they have no known competing financial interests or personal relationships that could have appeared to influence the work reported in this paper.

Acknowledgements

Jatin Kala was supported by an Australian Research Council Discovery Early Career Researcher Award (DE170100102). This research/project was undertaken with the assistance of resources and services from the National Computational Infrastructure (NCI), which is supported by the Australian Government. Part of the post-processing of model outputs was carried out on the PAWSEY Supercomputing Centre Nimbus flexible and fast high-throughput computing infrastructure. Annette L. Hirsch is supported by the Australian Research Council Centre of Excellence for Climate Extremes (CE170100023). We thank Professor Andrew J. Pitman for providing critical comments on earlier drafts of the manuscript. The comments of an anonymous reviewer and the editor in chief, Lisa Alexander, helped to improve the manuscript. All of this assistance is gratefully acknowledged.

Appendix A. Supplementary data

Supplementary data to this article can be found online at https://doi.org/10.1016/j.wace.2020.100282.

References

Allen, M.R., Dube, O.P., Solecki, W., Aragón-Durand, F., Cramer, W., Humphreys, S., Kainuma, M., Kala, J., Mahowald, N., Mulugetta, Y., Perez, R., Wairiu, M., Zickfeld, K., 2018. Framing and context. In: Global Warming of 1.5°C. An IPCC Special Report on the Impacts of Global Warming of 1.5°C above Pre-industrial Levels and Related Global Greenhouse Gas Emission Pathways, in the Context of Strengthening the Global Response to the.

Andrys, J., Kala, J., Lyons, T.J., 2017. Regional climate projections of mean and extreme climate for the southwest of Western Australia (1970–1999 compared to 2030–2059). Clim. Dynam. 48, 1723–1747. https://doi.org/10.1007/s00382-016-3169-5.

Andrys, J., Lyons, T.J., Kala, J., 2016. Evaluation of a WRF ensemble using GCM boundary conditions to quantify mean and extreme climate for the southwest of Western Australia (1970-1999). Int. J. Climatol. 36, 4406–4424. https://doi.org/10.1002/joc.4641.

Andrys, J., Lyons, T.J., Kala, J., 2015. Multidecadal evaluation of WRF downscaling capabilities over western Australia in simulating rainfall and temperature extremes. J. Appl. Meteorol. Climatol. 54, 370–394. https://doi.org/10.1175/JAMC-D-14-0212.1.

Arblaster, J.M., Alexander, L.V., 2012. The impact of the El Niño-Southern Oscillation on maximum temperature extremes. Geophys. Res. Lett. 39 https://doi.org/10.1029/2012GL053409.

Australian Bureau of Statistics, 2018. Land Management and Farming in Australia, pp. 2016–2017 [WWW Document].

Australian Bureau of Statistics, 2008. Water and the Murray-Darling Basin - A Statistical Profile, 2000-01 to 2005-06 [WWW Document].

Betts, A.K., Miller, M.J., 1986. A new convective adjustment scheme. Part II: single column tests using GATE wave, BOMEX, ATEX and arctic air-mass data sets. Q. J. R. Meteorol. Soc. 112, 693–709. https://doi.org/10.1002/qj.49711247308.

Boisier, J.P., de Noblet-Ducoudré, N., Pitman, A.J., Cruz, F.T., Delire, C., van den Hurk, B.J.J.M., van der Molen, M.K., Müller, C., Voldoire, A., 2012. Attributing the impacts of land-cover changes in temperate regions on surface temperature and heat fluxes to specific causes: results from the first LUCID set of simulations. J. Geophys. Res. Atmos. 117 https://doi.org/10.1029/2011JD017106.

Breuer, L., Eckhardt, K., Frede, H.-G., 2003. Plant parameter values for models in temperate climates. Ecol. Model. 169, 237–293. https://doi.org/10.1016/S0304-3800(03)00274-6.

Chen, F., Dudhia, J., 2001. Coupling an advanced land surface–hydrology model with the penn state–NCAR MM5 modeling system. Part II: preliminary model validation. Mon. Weather Rev. 129, 587–604. https://doi.org/10.1175/1520-0493(2001)129<0587:CAALSH>2.0.CO, 2.

Cowan, T., Purich, A., Perkins, S., Pezza, A., Boschat, G., Sadler, K., 2014. More frequent, longer, and hotter heat waves for Australia in the twenty-first century. J. Clim. 27, 5851–5871. https://doi.org/10.1175/JCLI-D-14-00092.1.

Dagon, K., Schrag, D.P., 2016. Exploring the effects of solar radiation management on water cycling in a coupled land–atmosphere model*. J. Clim. 29, 2635–2650. https://doi.org/10.1175/JCLI-D-15-0472.1.

Davin, E.L., Seneviratne, S.I., Ciais, P., Olioso, A., Wang, T., 2014. Preferential cooling of hot extremes from cropland albedo management. Proc. Natl. Acad. Sci. Unit. States Am. 111, 9757–9761. https://doi.org/10.1073/pnas.1317323111.

de Noblet-Ducoudré, N., Boisier, J.-P., Pitman, A., Bonan, G.B., Brovkin, V., Cruz, F., Delire, C., Gayler, V., van den Hurk, B.J.J.M., Lawrence, P.J., van der Molen, M.K., Müller, C., Reick, C.H., Strengers, B.J., Voldoire, A., 2012. Determining robust impacts of land-use-induced land cover changes on surface climate over North America and Eurasia: results from the first set of LUCID experiments. J. Clim. 25, 3261–3281. https://doi.org/10.1175/JCLI-D-11-00338.1.

Dee, D.P., Uppala, S.M., Simmons, A.J., Berrisford, P., Poli, P., Kobayashi, S., Andrae, U., Balmaseda, M.A., Balsamo, G., Bauer, P., Bechtold, P., Beljaars, A.C.M., van de Berg, L., Bidlot, J., Bormann, N., Delsol, C., Dragani, R., Fuentes, M., Geer, A.J., Haimberger, L., Healy, S.B., Hersbach, H., Hólm, E.V., Isaksen, L., Kållberg, P., Köhler, M., Matricardi, M., McNally, A.P., Monge-Sanz, B.M., Morcrette, J.-J., Park, B.-K., Peubey, C., de Rosnay, P., Tavolato, C., Thépaut, J.-N., Vitart, F., 2011. The ERA-Interim reanalysis: configuration and performance of the data assimilation system. Q. J. R. Meteorol. Soc. 137, 553–597. https://doi.org/10.1002/qj.828.

Di Virgilio, G., Evans, J.P., Di Luca, A., Olson, R., Argüeso, D., Kala, J., Andrys, J., Hoffmann, P., Katzfey, J.J., Rockel, B., 2019. Evaluating reanalysis-driven CORDEX regional climate models over Australia: model performance and errors. Clim. Dynam. https://doi.org/10.1007/s00382-019-04672-w.

Dirmeyer, P.A., 2011. The terrestrial segment of soil moisture-climate coupling. Geophys. Res. Lett. 38 https://doi.org/10.1029/2011GL048268 n/a-n/a.

Doughty, C.E., Field, C.B., McMillan, A.M.S., 2011. Can crop albedo be increased through the modification of leaf trichomes, and could this cool regional climate? Climatic Change 104, 379–387. https://doi.org/10.1007/s10584-010-9936-0.

Dudhia, J., 1989. Numerical study of convection observed during the winter monsoon experiment using a mesoscale two-dimensional model. J. Atmos. Sci. 46, 3077–3107. https://doi.org/10.1175/1520-0469(1989)046<3077:NSOCOD>2.0.CO, 2.

Evans, J.P., Ekström, M., Ji, F., 2012. Evaluating the performance of a WRF physics ensemble over South-East Australia. Clim. Dynam. 39, 1241–1258. https://doi.org/10.1007/s00382-011-1244-5.

Evans, J.P., McCabe, M.F., 2010. Regional climate simulation over Australia's Murray-Darling basin: a multitemporal assessment. J. Geophys. Res. 115, 1–15. https://doi.org/10.1029/2010JD013816.

Febrero, A., Fernandez, S., Molina-Cano, J.L., Araus, J.L., 1998. Yield, carbon isotope discrimination, canopy reflectance and cuticular conductance of barley isolines of differing glaucousness. J. Exp. Bot. 49, 1575–1581. https://doi.org/10.1093/jxb/49.326.1575.

Firth, R., Kala, J., Lyons, T.J., Andrys, J., 2017. An analysis of regional climate simulations for western Australia's wine regions—model evaluation and future climate projections. J. Appl. Meteorol. Climatol. 56, 2113–2138. https://doi.org/10.1175/JAMC-D-16-0333.1.

Friedlingstein, P., Andrew, R.M., Rogelj, J., Peters, G.P., Canadell, J.G., Knutti, R., Luderer, G., Raupach, M.R., Schaeffer, M., van Vuuren, D.P., Le Quéré, C., 2014. Persistent growth of CO2 emissions and implications for reaching climate targets. Nat. Geosci. 7, 709–715. https://doi.org/10.1038/ngeo2248.

Gentilli, J., 1971. Climates of Australia and New Zealand. Elsevier.

Goes, M., Tuana, N., Keller, K., 2011. The economics (or lack thereof) of aerosol geoengineering. Climatic Change 109, 719–744. https://doi.org/10.1007/s10584-010-9961-z.

Grant, R.H., Heisler, G.M., Gao, W., Jenks, M., 2003. Ultraviolet leaf reflectance of common urban trees and the prediction of reflectance from leaf surface characteristics. Agric. For. Meteorol. 120, 127–139. https://doi.org/10.1016/j.agrformet.2003.08.025.

Hatfield, J.L., Carlson, R.E., 1979. Light quality distributions and spectral albedo of three maize canopies. Agric. Meteorol. 20, 215–226. https://doi.org/10.1016/0002-1571(79)90022-0.

Henley, B.J., King, A.D., 2017. Trajectories toward the 1.5°C Paris target: modulation by the interdecadal pacific oscillation. Geophys. Res. Lett. 44, 4256–4262. https://doi.org/10.1002/2017GL073480.

Hirsch, A.L., Evans, J.P., Di Virgillio, G., Perkins-Kirkpatrick, S.E., Argüeso, D., Pitman, A.J., Carouge, C.C., Kala, J., Andrys, J., Petrelli, P., Rockel, B., 2019a. Amplification of Australian heatwaves via local land-atmosphere coupling. J. Geophys. Res. Atmos. 2019JD030665. https://doi.org/10.1029/2019JD030665.

Hirsch, A.L., Kala, J., Carouge, C.C., De Kauwe, M.G., Di Virgilio, G., Ukkola, A.M., Evans, J.P., Abramowitz, G., 2019b. Evaluation of the CABLEv2.3.4 land surface model coupled to NU-WRFv3.9.1.1 in simulating temperature and precipitation

means and extremes over CORDEX AustralAsia within a WRF physics ensemble. J. Adv. Model. Earth Syst. 2019MS001845. https://doi.org/10.1029/2019MS001845.
Hirsch, A.L., Kala, J., Carouge, C.C., De Kauwe, M.G., Di Virgilio, G., Ukkola, A.M., Evans, J.P., Abramowitz, G., 2019c. Evaluation of the CABLEv2.3.4 land surface model coupled to NU-WRFv3.9.1.1 in simulating temperature and precipitation means and extremes over CORDEX AustralAsia within a WRF physics ensemble. J. Adv. Model. Earth Syst. 2019MS001845. https://doi.org/10.1029/2019MS001845.
Hirsch, A.L., Pitman, A.J., Kala, J., 2014. The role of land cover change in modulating the soil moisture-temperature land-atmosphere coupling strength over Australia. Geophys. Res. Lett. 41, 5883–5890. https://doi.org/10.1002/2014GL061179.
Hirsch, A.L., Pitman, A.J., Kala, J., Lorenz, R., Donat, M.G., 2015a. Modulation of land-use change impacts on temperature extremes via land–atmosphere coupling over Australia. Earth Interact. 19, 1–24. https://doi.org/10.1175/EI-D-15-0011.1.
Hirsch, A.L., Pitman, A.J., Kala, J., Lorenz, R., Donat, M.G., 2015b. Modulation of land-use change impacts on temperature extremes via land–atmosphere coupling over Australia. Earth Interact. 19, 1–24. https://doi.org/10.1175/EI-D-15-0011.1.
Hirsch, A.L., Prestele, R., Davin, E.L., Seneviratne, S.I., Thiery, W., Verburg, P.H., 2018. Modelled biophysical impacts of conservation agriculture on local climates. Global Change Biol. 24, 4758–4774. https://doi.org/10.1111/gcb.14362.
Hirsch, A.L., Wilhelm, M., Davin, E.L., Thiery, W., Seneviratne, S.I., 2017. Can climate-effective land management reduce regional warming? J. Geophys. Res. Atmos. 122, 2269–2288. https://doi.org/10.1002/2016JD026125.
Hong, S.-Y., Noh, Y., Dudhia, J., 2006. A new vertical diffusion package with an explicit treatment of entrainment processes. Mon. Weather Rev. 134, 2318–2341. https://doi.org/10.1175/MWR3199.1.
Imran, H.M., Kala, J., Ng, A.W.M., Muthukumaran, S., 2019. Effectiveness of vegetated patches as Green Infrastructure in mitigating Urban Heat Island effects during a heatwave event in the city of Melbourne. Weather Clim. Extrem. 25, 100217. https://doi.org/10.1016/j.wace.2019.100217.
Imran, H.M., Kala, J., Ng, A.W.M., Muthukumaran, S., 2018. Effectiveness of green and cool roofs in mitigating urban heat island effects during a heatwave event in the city of Melbourne in southeast Australia. J. Clean. Prod. 197, 393–405. https://doi.org/10.1016/j.jclepro.2018.06.179.
Irvine, P.J., Kravitz, B., Lawrence, M.G., Muri, H., 2016. An overview of the Earth system science of solar geoengineering. Wiley Interdiscip. Rev. Clim. Chang. 7, 815–833. https://doi.org/10.1002/wcc.423.
Jacobs, S.J., Gallant, A.J.E., Tapper, N.J., Li, D., 2018. Use of cool roofs and vegetation to mitigate urban heat and improve human thermal stress in melbourne, Australia. J. Appl. Meteorol. Climatol. 57, 1747–1764. https://doi.org/10.1175/JAMC-D-17-0243.1.
Janjić, Z.I., 1994. The step-mountain eta coordinate model: further developments of the convection, viscous sublayer, and turbulence closure schemes. Mon. Weather Rev. 122, 927–945. https://doi.org/10.1175/1520-0493(1994)122<0927:TSMECM>2.0.CO;2.
Kain, J.S., 2004. The kain–fritsch convective parameterization: an update. J. Appl. Meteorol. 43, 170–181. https://doi.org/10.1175/1520-0450(2004)043<0170:TKCPAU>2.0.CO, 2.
Kala, J., Andrys, J., Lyons, T.J., Foster, I.J., Evans, B.J., 2015a. Sensitivity of WRF to driving data and physics options on a seasonal time-scale for the southwest of Western Australia. Clim. Dynam. 44, 633–659. https://doi.org/10.1007/s00382-014-2160-2.
Kala, J., Evans, J.P., Pitman, A.J., 2015b. Influence of antecedent soil moisture conditions on the synoptic meteorology of the Black Saturday bushfire event in southeast Australia. Q. J. R. Meteorol. Soc. 141, 3118–3129. https://doi.org/10.1002/qj.2596.
Kala, J., Tenna, A.S., Rudloff, D., Andrys, J., Rieke, O., Lyons, T.J., 2020. Evaluation of the Weather Research and Forecasting model in simulating fire weather for the south-west of Western Australia. Int. J. Wildland Fire. https://doi.org/10.1071/WF19111.
Keith, D.W., 2000. Geoengineering the climate: history and prospect. Annu. Rev. Energy Environ. 25, 245–284. https://doi.org/10.1146/annurev.energy.25.1.245.
King, A.D., Karoly, D.J., Henley, B.J., 2017. Australian climate extremes at 1.5°C and 2°C of global warming. Nat. Clim. Change 7, 412–416. https://doi.org/10.1038/nclimate3296.
Kravitz, B., Robock, A., Boucher, O., Schmidt, H., Taylor, K.E., Stenchikov, G., Schulz, M., 2011. The geoengineering model Intercomparison project (GeoMIP). Atmos. Sci. Lett. 12, 162–167. https://doi.org/10.1002/asl.316.
Lavin-Gullon, A., Fernandez, J., Bastin, S., Cardoso, R.M., Fita, L., Giannaros, T.M., Goergen, K., Gutierrez, J.M., Kartsios, S., Katragkou, E., Lorenz, T., Milovac, J., Soares, P.M.M., Sobolowski, S., Warrach-Sagi, K., 2020. Internal variability versus multi-physics uncertainty in a regional climate model. Int. J. Climatol. n/a. https://doi.org/10.1002/joc.6717.
Lu, Y., Williams, I.N., Bagley, J.E., Torn, M.S., Kueppers, L.M., 2017. Representing winter wheat in the community land model (version 4.5). Geosci. Model Dev. (GMD) 10, 1873–1888. https://doi.org/10.5194/gmd-10-1873-2017.
Ma, S., Goldstein, M., Pitman, A.J., Haghdadi, N., MacGill, I., 2017. Pricing the urban cooling benefits of solar panel deployment in Sydney, Australia. Sci. Rep. 7, 43938. https://doi.org/10.1038/srep43938.
Mac Dowell, N., Fennell, P.S., Shah, N., Maitland, G.C., 2017. The role of CO2 capture and utilization in mitigating climate change. Nat. Clim. Change 7, 243–249. https://doi.org/10.1038/nclimate3231.
McEvoy, D., Ahmed, I., Mullett, J., 2012. The impact of the 2009 heat wave on Melbourne's critical infrastructure. Local Environ. 17, 783–796. https://doi.org/10.1080/13549839.2012.678320.
Mlawer, E.J., Taubman, S.J., Brown, P.D., Iacono, M.J., Clough, S.A., 1997. Radiative transfer for inhomogeneous atmospheres: RRTM, a validated correlated-k model for the longwave. J. Geophys. Res. Atmos. 102, 16663–16682. https://doi.org/10.1029/97JD00237.
Parker, A., Irvine, P.J., 2018. The risk of termination shock from solar geoengineering. Earth's Futur 6, 456–467. https://doi.org/10.1002/2017EF000735.
Peng, Bi, Williams, S., Loughnan, M., Lloyd, G., Hansen, A., Kjellstrom, T., Dear, K., Saniotis, A., 2011. The effects of extreme heat on human mortality and morbidity in Australia: implications for public health. Asia Pac. J. Publ. Health 23, 27S–36S. https://doi.org/10.1177/1010539510391644.
Perkins-Kirkpatrick, S.E., White, C.J., Alexander, L.V., Argüeso, D., Boschat, G., Cowan, T., Evans, J.P., Ekström, M., Oliver, E.C.J., Phatak, A., Purich, A., 2016. Natural hazards in Australia: heatwaves. Climatic Change 139, 101–114. https://doi.org/10.1007/s10584-016-1650-0.
Perkins, S.E., Alexander, L.V., Nairn, J.R., 2012. Increasing frequency, intensity and duration of observed global heatwaves and warm spells. Geophys. Res. Lett. 39 https://doi.org/10.1029/2012GL053361, 2012GL053361.
Piggin, I., Schwerdtfeger, P., 1973. Variations in the albedo of wheat and barley crops. Arch. für Meteorol. Geophys. und Bioklimatologie Ser. B 21, 365–391. https://doi.org/10.1007/BF02253314.
Pongratz, J., Lobell, D.B., Cao, L., Caldeira, K., 2012. Crop yields in a geoengineered climate. Nat. Clim. Change 2, 101.
Preston, C.J., 2013. Ethics and geoengineering: reviewing the moral issues raised by solar radiation management and carbon dioxide removal. Wiley Interdiscip. Rev. Clim. Chang. 4, 23–37. https://doi.org/10.1002/wcc.198.
Ramankutty, N., Evan, A.T., Monfreda, C., Foley, J.A., 2008. Farming the planet: 1. Geographic distribution of global agricultural lands in the year 2000. Global Biogeochem. Cycles 22. https://doi.org/10.1029/2007GB002952 n/a-n/a.
Ridgwell, A., Singarayer, J.S., Hetherington, A.M., Valdes, P.J., 2009. Tackling regional climate change by leaf albedo bio-geoengineering. Curr. Biol. 19, 146–150. https://doi.org/10.1016/j.cub.2008.12.025.
Robock, A., Marquardt, A., Kravitz, B., Stenchikov, G., 2009. Benefits, risks, and costs of stratospheric geoengineering. Geophys. Res. Lett. 36, L19703. https://doi.org/10.1029/2009GL039209.
Rogelj, J., Elzen, M. Den, Fransen, T., Fekete, H., Winkler, H., Schaeffer, R., Sha, F., Riahi, K., Meinshausen, M., 2016. Paris Agreement climate proposals need boost to keep warming well below 2°C. Nat. Clim. Change 534, 631–639. https://doi.org/10.1038/nature18307.
Ruthrof, K.X., Breshears, D.D., Fontaine, J.B., Froend, R.H., Matusick, G., Kala, J., Miller, B.P., Mitchell, P.J., Wilson, S.K., van Keulen, M., Enright, N.J., Law, D.J., Wernberg, T., Hardy, G.E.S.J., 2018. Subcontinental heat wave triggers terrestrial and marine, multi-taxa responses. Sci. Rep. 8, 13094. https://doi.org/10.1038/s41598-018-31236-5.
Seneviratne, S.I., Phipps, S.J., Pitman, A.J., Hirsch, A.L., Davin, E.L., Donat, M.G., Hirschi, M., Lenton, A., Wilhelm, M., Kravitz, B., 2018. Land radiative management as contributor to regional-scale climate adaptation and mitigation. Nat. Geosci. 11, 88–96. https://doi.org/10.1038/s41561-017-0057-5.
Skamarock, W.C., Klemp, J.B., Dudhia, J., Gill, D.O., Liu, Z., Berner, J., Wang, W., Powers, J.G., Duda, M.G., Barker, D.M., Huang, X.-Y., 2019. A Description of the Advanced Research WRF Version 4. NCAR Tech. Note NCAR/TN-556+STR, p. 145. https://doi.org/10.5065/1dfh-6p97.
Uddin, M.N., Marshall, D.R., 1988. Variation in epicuticular wax content in wheat. Euphytica 38, 3–9. https://doi.org/10.1007/BF00024805.
van Dijk, A.I.J.M., Beck, H.E., Crosbie, R.S., de Jeu, R.A.M., Liu, Y.Y., Podger, G.M., Timbal, B., Viney, N.R., 2013. The Millennium Drought in southeast Australia (2001-2009): natural and human causes and implications for water resources, ecosystems, economy, and society. Water Resour. Res. 49, 1040–1057. https://doi.org/10.1002/wrcr.20123.
Vaughan, N.E., Lenton, T.M., 2011. A review of climate geoengineering proposals. Climatic Change 109, 745–790. https://doi.org/10.1007/s10584-011-0027-7.
Wilhelm, M., Davin, E.L., Seneviratne, S.I., 2015. Climate engineering of vegetated land for hot extremes mitigation: an Earth system model sensitivity study. J. Geophys. Res. Atmos. 120, 2612–2623. https://doi.org/10.1002/2014JD022293.
Wilkinson, I., 2019. Western Australian Wheat Industry [WWW Document]. URL, 7.31.19. https://www.agric.wa.gov.au/grains-research-development/western-australian-wheat-industry.